INSTABILITIES AND FILAMENTATION OF DISPERSIVE ALFVÉN WAVES

D. LAVEDER, T. PASSOT AND P.L. SULEM

CNRS UMR 6529, Observatoire de la Côte d'Azur
BP 4229, 06304 Nice Cedex 4, France
E-mail:sulem@obs-nice.fr

Direct numerical simulations of the three-dimensional Hall-MHD equations and of a long-wavelength asymptotic model are used to study the instabilities and the nonlinear dynamics of a circularly polarized Alfvén wave subject to a weak random noise. The evolution is shown to be strongly sensitive to the spectral extension of the initial noise, due to the presence of competing instabilities. The formation of magnetic filaments is usually observed when only large-scale modulational perturbations are permitted, while a more turbulent picture is obtained when small-scale unstable modes are initially excited. A filamentary dynamics nevertheless develops in the presence of a broad initial spectrum in the case of a right-hand polarized pump of long wavelength.

1 Introduction

The magnetohydrodynamic (MHD) description of magnetized plasmas concentrates on length scales that are much longer than the ion inertial length c/ω_{pi}, defined as the ratio of the light velocity to the ion plasma frequency, and time scales much larger than the inverse ion gyromagnetic frequency Ω_i^{-1}. When dealing with phenomena whose characteristic scales approach these limits, the Hall term that originates from the ion inertia becomes relevant in the generalized Ohm's law. In the absence of significant dissipation, the dynamics is then governed by the Hall-MHD equations[1]

$$\partial_t \rho + \nabla \cdot (\rho \mathbf{u}) = 0 \tag{1}$$

$$\rho(\partial_t \mathbf{u} + \mathbf{u} \cdot \nabla \mathbf{u}) = -\frac{\beta}{\gamma} \nabla \rho^\gamma + (\nabla \times \mathbf{b}) \times \mathbf{b} \tag{2}$$

$$\partial_t \mathbf{b} - \nabla \times (\mathbf{u} \times \mathbf{b}) = -\frac{1}{R_i} \nabla \times \Big(\frac{1}{\rho} (\nabla \times \mathbf{b}) \times \mathbf{b} \Big) \tag{3}$$

$$\nabla \cdot \mathbf{b} = 0. \tag{4}$$

As usual, ρ is the density of the plasma, $\mathbf{u}$ its velocity and $\mathbf{b}$ the magnetic field. The equations are written in a non-dimensional form, taking as unity the Alfvén speed $c_A = \mathcal{B}_0/\sqrt{4\pi\rho_0}$, where $\mathcal{B}_0$ is the magnitude of the ambient magnetic field and ρ_0 the mean density of the plasma. Furthermore, $\beta = c_s^2/c_A^2$, where c_s is the sound velocity, γ is the polytropic gas constant and

$R_i = \Omega_i L/c_A$, where L is a reference length, denotes the non-dimensional ion-cyclotron frequency.

In the presence of an ambient magnetic field taken in the x-direction, the Hall-MHD equations admit special solutions, named after Ferraro,[2] in the form of finite-amplitude circularly-polarized Alfvén waves $b_y - i\sigma b_y = B_0 e^{i(kx-\omega t)}$ propagating along the magnetic field with, for forward propagation, a dispersion relation $\omega = \frac{\sigma k^2}{2R_i} + k\sqrt{1+\left(\frac{k}{2R_i}\right)^2}$ where $\sigma = +1$ or -1, depending on right-hand or left-hand polarization. An important issue concerns the instabilities that can affect such pump waves and the forthcoming nonlinear dynamics that can lead to small-scale formation and heating of the plasma. For purely longitudinal perturbations, the problem becomes one-dimensional and was extensively studied. Depending on the situation, solitonic structures, envelope solitons or a turbulent cascade are obtained.[3]

Another special case corresponds to the effect of transverse perturbations. For small amplitude waves, the problem is amenable to a multiple-scale analysis leading to a two-dimensional nonlinear Schrödinger (NLS) equation[4] for the pump envelope that, in some instances, predicts wave collapse and formation of intense magnetic filaments (Alfvén-wave filamentation).[5−7]

When scale separation does not hold, as a consequence of a finite-amplitude wave or of instabilities at the scale of the pump, the problem is to be addressed by numerical simulations. It nevertheless simplifies when the Alfvén wave is considered in the long-wavelength limit. By means of a reductive perturbative expansion, the Hall-MHD equations then lead to long-wave asymptotic equations that can be viewed as a three-dimensional generalization[8,9] of the derivative nonlinear Schrödinger (DNLS) equation[10−14], including the coupling to the magnetosonic waves averaged along the direction of propagation. These equations provide in particular a description of transverse collapse in the case of finite amplitude Alfvén waves where filamentation is replaced by the formation of "magnetic pancakes" with moderate amplification of the wave amplitude but development of strong gradients.[15]

Simulations are presented here for various regimes of parameters. The algorithms used for the three-dimensional Hall-MHD and DNLS equations are based on a Fourier spectral method and a third-order Runge-Kutta time stepping discussed in the appendix. In all the simulations we used $c_A/\Omega_i = c/\omega_{pi}$ as the reference scale L, which implies $R_i = 1$. A main observation is the sensitivity of the nonlinear dynamics not only to the characteristics of the pump wave but also, because of the presence of various competing instabilities, to the spectral extension of the initial perturbating noise.

2 The special case of the longitudinal dynamics

A first illustration of the multiplicity of regimes developed by dispersive Alfvén waves propagating along the ambient field is already obtained in one space-dimension. In the plane (k, β), the ranges of existence of the various linear instabilities affecting a small-amplitude circularly polarized pump of wavenumber k appear to be delimited by the resonances associated with the equality

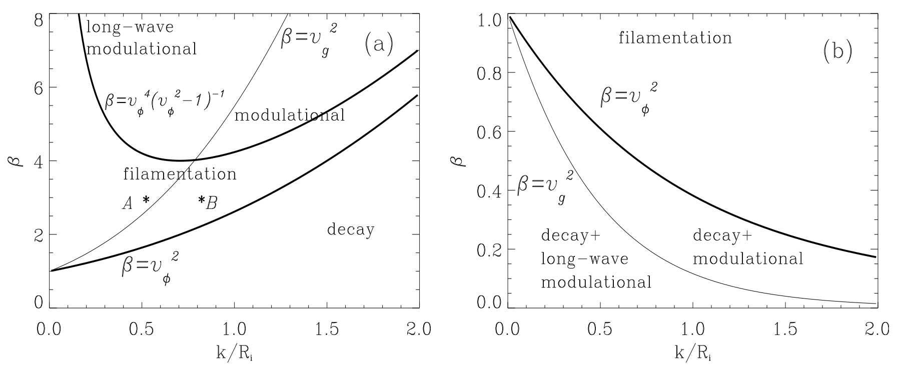

Figure 1. Instability regions in the plane (β, k) for a small-amplitude Alfvén wave with right-hand (a) or left-hand (b) polarization. Thick lines delimit the domains of the filamentation instability. Points A and B correspond to typical conditions in forthcoming numerical simulations.

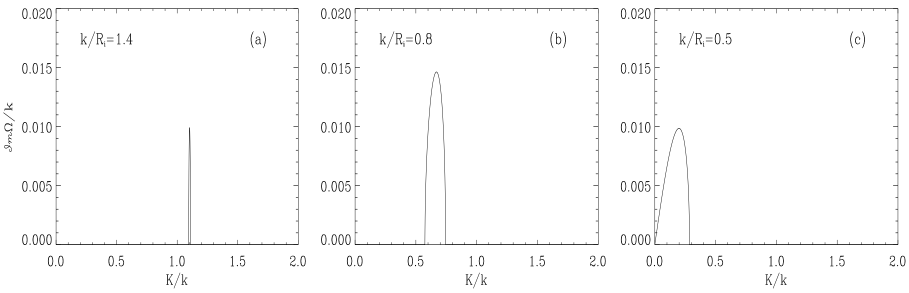

Figure 2. Growth rate versus perturbation wavenumber (both normalized by the pump wavenumber k) for examples of decay (a), modulational (b) and long-wavelength modulational (c) instabilities, for a right-hand polarized wave when $\beta = 2.7$.

of the sound speed (given by $\sqrt{\beta}$ when the Alfvén velocity is taken as unity) with the group or phase velocities v_g or v_ϕ of the Alfvén wave[16] (Figs. 1). Note that different instabilities can coexist in the case of a left-hand polarized wave. As exemplified in Fig. 2a, decay instability affects wavenumbers larger than the pump wavenumber k, while the instability is said modulational in the Alfvén-wave literature[17] when the unstable wavenumbers are smaller than k (Fig. 2b). The rescaling by the pump wavenumber in Fig. 2 is suggested by the fact that for a wave perturbation of the form $e^{i[(k\pm K)x-(\omega\pm\Omega)t]}$, the dispersion relation implies that Ω/k depends on K/k and k/R_i. In the special case of a "long-wavelength" modulational instability that extends down to the zero wavenumber (Fig. 2c), the forthcoming nonlinear dynamics is amenable to a multiple-scale analysis that leads to a nonlinear Schrödinger (NLS) equation

$$i\partial_\tau B + \frac{\omega''}{2}\partial_{\xi\xi}B + \frac{k v_g}{4(\beta - v_g^2)}|B|^2 B = 0. \tag{5}$$

This equation describes in terms of the stretched variables $\xi = \epsilon(x - v_g t)$ and $\tau = \epsilon^2 t$, the evolution of the Alfvén wave amplitude defined, up to subdominant harmonics, by $b_y - i\sigma b_z = \epsilon B e^{i(kx-\omega t)}$ with $\sigma = -1$ for left-hand polarization and $\sigma = +1$ for right-hand polarization. In one space dimension, the cubic NLS equation is integrable and predicts the formation of envelope solitons. In contrast, when the instability takes place at smaller scales (Figs. 2b and 2c), the coupling to the magneto-sonic waves plays an important role, leading to strong nonlinear phenomena with formation of density shocks.

When the pump wavenumber k is decreased to order ϵ^2, while the wave amplitude is kept of order ϵ, the dispersion becomes comparable to the nonlinearity and the dynamics is no longer governed by an envelope equation. It is nevertheless amenable to a reductive perturbative expansion which, for $\beta \neq 1$, selects the Alfvén waves. To leading order, they are governed by the previously mentioned DNLS equation for the transverse magnetic field $b_y + ib_z = \epsilon b$

$$\partial_\tau b + \frac{1}{4(1-\beta)}\partial_\xi\Big((|b|^2 - \langle|b|^2\rangle)b\Big) + \frac{i}{2R_i}\partial_{\xi\xi}b = 0, \tag{6}$$

where the brackets indicate averaging along the direction of propagation. The stretched variables are defined as $\xi = \epsilon^2(x - t)$ and $\tau = \epsilon^4 t$. Like many other long-wavelength equations (Korteweg-de Vries, Benjamin-Ono, $\cdots$), the DNLS equation is a soliton equation integrable by inverse scattering.[18] It involves a complex field because of the degeneracy associated with the equality in the dispersionless limit of the phase velocity of the Alfvén and fast ($\beta < 1$) or slow ($\beta > 1$) magnetosonic waves in the case of propagation along the

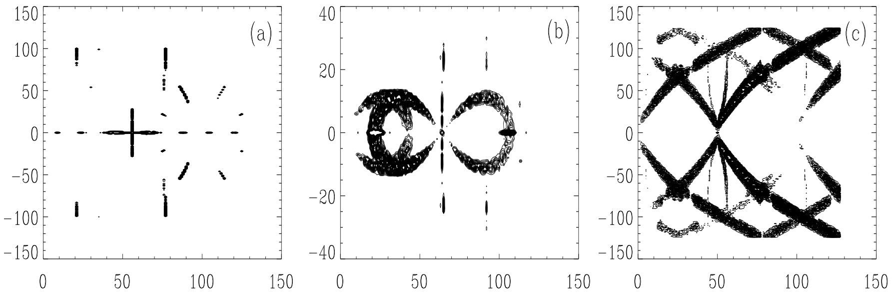

Figure 3. Spectral instability range as delimited by b_y Fourier modes contours (similar picture with b_z) obtained by two-dimensional numerical simulations of Hall-MHD equations, for a small-amplitude right-hand polarized Alfvén wave with $k = 0.5$ (a) or $k = 0.8$ (b) both for $\beta = 2.7$, and for a left-hand polarized wave with $k = 1$ when $\beta = 1.5$. The (positive) longitudinal and transverse wavenumbers are measured in units of $\Delta k_{\|} = 1/112$ (a), 1/80 (b), 1/50 (c) and $\Delta k_{\perp} = 1/72$ (a), 1/96 (b), 1/28 (c).

ambient field. It is convenient to introduce a parameter ν, measuring the relative magnitude of the dispersion compared to the nonlinearity. For this purpose, denoting by b_0 and k^{-1} the initial typical amplitude and (longitudinal) wavelength of the transverse magnetic field, we rescale b by b_0, the longitudinal coordinate by k^{-1} and the time by $(kb_0^2)^{-1}$. In eq. (6) the coefficient $\frac{1}{2R_i}$ is then replaced by $\nu = \frac{k}{2R_i b_0^2}$. In the limit of large ν (very small amplitude wave), the dispersion is dominant and a multiple-scale analysis performed on the DNLS equation reproduces the NLS equation (5) where the coefficients are taken in the limit $k \to 0$. The DNLS equation that does not retain counter-propagating waves cannot however describe the decay instability (that survives in the long-wavelength limit) and is thus restricted to plasmas with $\beta > 1$. In this case, quantitative comparisons with the direct numerical simulations[16] show a satisfactory agreement on times that scale like ϵ^{-4}, which validates the asymptotics.

3 Multidimensional linear instabilities

The longitudinal instabilities displayed in Figs. 1 and 2 have multidimensional extensions and coexist with transverse and oblique instabilities, as seen on Figs. 3 for a right-hand polarized wave in typical conditions corresponding to points A ($k = 0.5$, $\beta = 2.7$) and B ($k = 0.8$, $\beta = 2.7$) of Fig. 1a and for left-hand polarization with $k = 1$ and $\beta = 1.5$. The instability ranges are obtained by short-time integrations of the Hall-MHD equations, restricted to two space dimensions because of the symmetry of the problem with respect to the direction of the transverse component of the perturbation wavevector. The nonlinear dynamics is in contrast sensitive to the presence of a third dimension.

As the pump wavenumber is reduced, the dynamics considerably slows down and it is convenient in this regime to use a three-dimensional extension of the DNLS equation discussed in Section 2. This long-wavelength limit involves a scaling of the transverse variables $\eta = \epsilon^3 y$, $\zeta = \epsilon^3 z$ and must include the coupling to mean fields (denoted by bars or brackets) resulting from the averaging of magneto-sonic waves along the direction of propagation[8,9]

$$\partial_\tau b + \partial_\xi \left(\frac{1}{2} bP + (\bar{u}_x + \frac{1}{2}\bar{b}_x) b \right) - \frac{1}{2}\partial_\perp P + \frac{i}{2R_i}\partial_{\xi\xi} b = 0 \tag{7}$$

$$\partial_\tau \bar{u}_x = \frac{1}{2}\left(\partial_\perp^* \langle bP \rangle + \partial_\perp \langle b^* P \rangle\right) \tag{8}$$

$$\partial_\xi \widetilde{b}_x + \frac{1}{2}\left(\partial_\perp^* b + \partial_\perp b^*\right) = 0. \tag{9}$$

In the above 3D-DNLS system, the notation $\partial_\perp = \partial_\eta + i\partial_\zeta$ has been introduced. Like the mean longitudinal velocity $\bar{u}_x$, the induced longitudinal magnetic field is rescaled by a factor ϵ and is separated in mean and fluctuating parts in the form $\bar{b}_x + \widetilde{b}_x$. Furthermore, $\bar{b}_x = -\frac{1}{1+\beta}(\frac{\langle |b|^2 \rangle}{2} - E_M)$ where the constant E_M, defined as the average over the whole domain of the magnetic energy density $\frac{|b|^2}{2}$, is retained to ensure that $\bar{b}_x$ is zero in one space dimension. The fluctuations of magnetic pressure are given by $P = \frac{1}{2(1-\beta)}(2\widetilde{b}_x + |b|^2 - \langle |b|^2 \rangle)$. By means of the same change of variables as in one dimension, together with the rescaling of the transverse coordinates by $(b_0 k)^{-1}$ and of the fields $\bar{u}_x$, $\bar{b}_x$, $\widetilde{b}_x$ by b_0^2, the coefficient $\frac{1}{2R_i}$ is replaced by the parameter ν in eq. (7). Numerical simulations of eqs. (7)–(9) show that the range of the unstable modes for a left-hand polarized pump in the long-wavelength limit remains qualitatively similar to that of Fig. 3c, with the persistence of significant oblique instabilities. In contrast, the spectral instability range strongly simplifies in the case of a right-hand pump and concentrates to large-scale modes in the purely transverse and longitudinal directions. In this case, for both large ($\nu = 50$) and moderate ($\nu = 0.5$) dispersion regimes, the growth rate in the transverse direction is dominant by about one order of magnitude when $\beta = 3$. As checked on direct numerical simulations of the Hall-MHD equations with decreasing pump wavenumber, the other instabilities are either suppressed or moved to scales that are too small to be retained by the DNLS asymptotics.

4 Transverse dynamics and filamentation

As already mentioned, a special attention was devoted to the transverse instability that affects low frequency modes and is amenable to a multiple-scale analysis leading to a two-dimensional NLS equation[6]

$$i\partial_\tau B + \alpha\Delta_\perp B - kv_g\Big(\frac{1}{v_g^2} - \frac{k^4}{4(\beta+1)\omega^4}\Big)|B|^2 B = 0. \tag{10}$$

Here the Laplacian is taken relatively to the stretched transverse variables $Y = \epsilon y$ and $Z = \epsilon z$. It follows that a right-hand polarized pump wave is unstable relatively to a long-wavelength transverse modulation (filamentation instability) when $v_\phi^2 < \beta < \frac{v_\phi^4}{v_\phi^2 - 1}$, while a left-hand polarized pump wave is unstable when $\beta > v_\phi^2$ (Figs. 1a–1b). In one dimension, the nonlinear saturation of the instability results in the formation of solitonic structures, while much more violent effects take place in two dimensions where the wave focuses transversally and collapses with a local blowup of the field B, associated with a breakdown of the multiple-scale asymptotics. In the primitive variables, this corresponds to the formation of intense magnetic filaments parallel to the ambient field. The question however arises of the relevance of the filamentation phenomenon in a context where the dynamics is not restricted to purely transverse instabilities. As seen on Figs. 3, the spectral ranges of the instabilities that develop for a pump of moderate wavenumber are rather extended and one may expect that the dynamics resulting from a competition of several instabilities will be sensitive to the characteristics of the initial noise.

As already noticed, the situation strongly simplifies in the DNLS description of a right-hand polarized pump, due to the absence of oblique instabilities. Numerical simulations of eqs. (7)–(9) in the strongly dispersive regime ($\nu = 50$) with a broad-spectrum initial noise show the formation of magnetic filaments.[19] In order to resolve the phenomenon of wave filamentation more accurately, in a context where only the transverse dynamics turns out to be relevant, we chose to present here simulations in a periodic box whose longitudinal extension equals the wavelength of the pump.[15] Figure 4a displays the filamentation that occurs for $\nu = 50$ when $\beta = 3$. The transverse cut presented in Fig. 4b shows that at the end of the simulation, the intensity $|b|^2$ has been locally amplified by two orders of magnitude. When the strength of the dispersion is reduced ($\nu = 0.5$), the transverse dynamics is no longer governed by the two-dimensional NLS equation. In this case, the amplification of the transverse magnetic field is only moderate and its intensity displays significant variations in the longitudinal direction, leading to the formation of magnetic structures with a pancake shape (Fig. 5a). Strong gradients develop

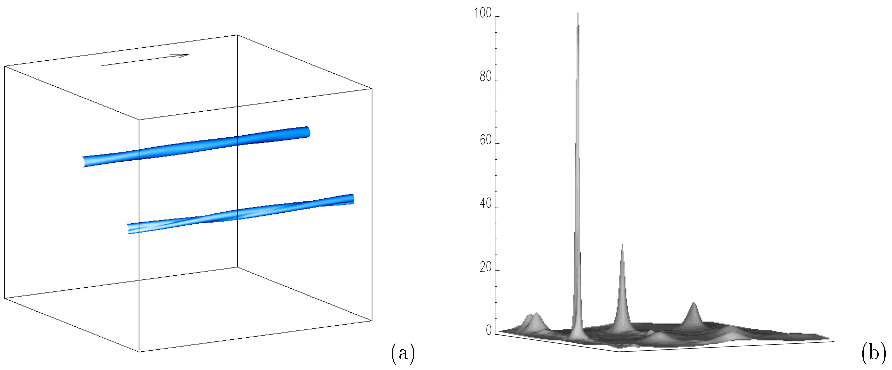

Figure 4. Magnetic filaments where $|b|^2$ exceeds its initial value by a factor 10 (a) and snapshot of $|b|^2$ in a plane transverse to the ambient field (b) in numerical simulations of the 3D-DNLS system with $\beta = 3$ and $\nu = 50$ at resolution 32×256^2. The arrow refers to the direction of the ambient magnetic field.

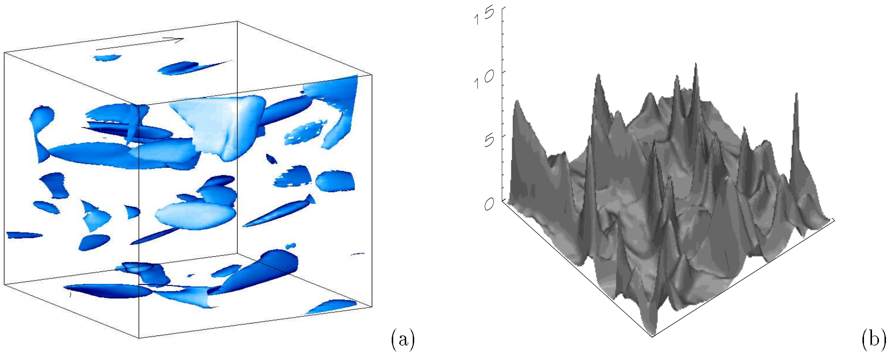

Figure 5. "Magnetic pancakes" where $|b|^2$ exceeds its initial value by a factor 4 (a) and snapshot of $|b|^2$ in a plane transverse to the ambient field (b) in numerical simulations of the 3D-DNLS system with $\beta = 3$ and $\nu = 0.5$ at resolution 32×128^2.

in planes transverse to the ambient field (Fig. 5b) and the question arises of the existence of a finite-time gradient singularity.

Still in the case of a right-hand polarized pump, it is of interest to consider the effect of increasing the wavenumber to moderate values (point A of Fig. 1a) for which the longitudinal modulational instability remains at large scale with nevertheless the presence of oblique instabilities at small scales (Fig. 3a). Direct numerical simulations of the Hall-MHD equations show that if small-scale modes are initially excited, they will prevent the formation of coherent magnetic structures (filaments or pancakes). Instead, small-scale structures are randomly scattered within the domain, with no significant amplification of the wave intensity. In contrast, when the initial perturbations are confined at sufficiently large scales, the oblique instabilities play no role and the dynamics, resulting from the competition of comparable large-scale transverse and longitudinal instabilities, leads to the formation of elongated structures where both the modulation associated with the longitudinal instability and the effect of the pump harmonics are visible (Fig. 6a).

When increasing further the pump wavenumber, the longitudinal instability no longer affects the largest scales but rather those comparable to the pump wavelength (point B of Fig. 1a). Two classes of perturbations are then considered. For an initial noise at scales large compared to that of the longitudinal instability, only large-scale oblique instabilities can compete with the transverse dynamics and filamentary structures weakly modulated by the corresponding oblique modes are visible (Fig. 6b). At the opposite, with a broad-spectrum perturbation, the dynamics is dominantly longitudinal with the formation of magnetic pancakes mostly transverse to the ambient field.

In the context of left-hand polarization, the presence of oblique insta-

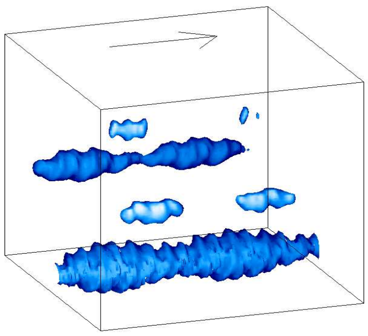

(a)

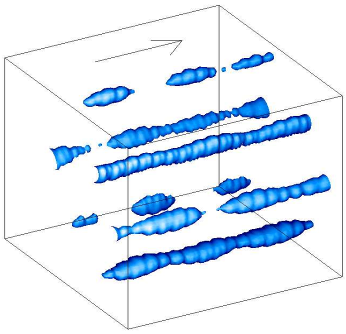

(b)

Figure 6. Regions where the transverse magnetic field intensity exceeds its initial value by a factor 4.5 in the conditions of point A (a) and by a factor 3.5 in the conditions of point B (b), resulting from the instability of an Alfvén wave of initial amplitude 0.1, in numerical simulation of Hall-MHD equations at resolution $128 \times (64)^2$.

bilities extending from large to small scales make the formation of magnetic filaments possible only with initial perturbations limited to very large scales.[19] Even in this case, the structures are significantly modulated and progressively destroyed as the initial spectrum is broadened.

Finally, as the wave amplitude is increased, one observes on the Hall-MHD simulations that, like in the DNLS limit, the intense magnetic filaments are replaced by magnetic pancakes of moderate amplitude.

5 Concluding remarks

The instabilities and the further nonlinear evolution of a circularly polarized Alfvén wave are analyzed in the context of Hall-MHD that retains dispersive effects due to ion inertia. The strong sensitivity of the dynamics to the spectral extension of the initial noise is in particular pointed out. Furthermore, the transverse collapse of a small-amplitude wave, leading to the formation of intense magnetic filaments parallel to the ambient field, is shown to be especially relevant for long-wavelength pumps with right-hand polarization, even in the presence of broad-spectrum perturbations that in other regimes may induce a more turbulent regime. Wave filamentation provides a mechanism for small scale formation that permits acceleration and heating of the plasma in a regime where no small-scale instabilities are present, and thus without requiring large-amplitude waves or inhomogeneity of the medium. Future developments should include the influence of finite ion Larmor radius [20,21] and the role of kinetic effects that are believed to be relevant when the parameter β exceeds unity. In one space dimension, a simple description of the latter effects in the long-wave limit is provided by additional nonlocal terms in the DNLS equation.[22−24]

Appendix: Numerical schemes

Both the three-dimensional Hall-MHD and DNLS equations are integrated using a pseudo-spectral method based on Fourier mode expansion. The dynamics being strongly sensitive to the linear instabilities that affect the system, a special attention is to be paid to the choice of the spatial discretization, in order to retain the most unstable modes. This may require the use of a computational box with different sizes in the longitudinal and transverse directions.

Concerning the time stepping, the Hall-MHD equations are solved with a low-storage Runge-Kutta scheme.[25] For the DNLS system, symbolically written

$$\frac{dU}{dt} = N(U) + L\,U,$$

the same scheme is used for the nonlinearities $N(U)$, while the Hall term $L\,U$ that in this case is linear and purely longitudinal, is treated exactly, using an exponential scheme. The transition from t_n to $t_{n+1} = t_n + \delta t$ is then given by

$$\begin{aligned} V_1 &= e^{\frac{1}{3}\delta t L}\left(U_n + \tfrac{1}{3}H_1\right) & \qquad H_1 &= \delta t N(U_n) \\ V_2 &= e^{\frac{5}{12}\delta t L}\left(V_1 + \tfrac{15}{16}H_2\right) & \qquad H_2 &= \delta t N(V_1) - \frac{5}{9}e^{\frac{1}{3}\delta t L}H_1 \\ U_{n+1} &= e^{\frac{1}{4}\delta t L}\left(V_2 + \tfrac{8}{15}H_3\right) & \qquad H_3 &= \delta t N(V_2) - \frac{153}{128}e^{\frac{5}{12}\delta t L}H_2. \end{aligned}$$

This numerical scheme is slightly dissipative, of an amount consistent with the $(\delta t)^3$-accuracy, which contributes to the numerical stability.

For the Hall-MHD equations, the maximal time step δt allowing numerical stability varies like N^{-2} in terms of the number N of collocation points in each direction. The integrations are also very time consuming due to the slow growth rate of the modulational instabilities, while the time step (typically $\delta t = 1.25 \cdot 10^{-3}$ for $N = 128$ in the conditions of our simulations that include a spherical truncation of the spectral domain) is constrained by stability conditions. As a consequence, the three-dimensional simulations were limited to this resolution.

We also checked on one-dimensional integrations, that with the time step retained for the above Runge-Kutta scheme, an Adams-Bashforth scheme would be unstable without the inclusion of extra dissipative terms leading to an overall dissipation larger than that obtained with the Runge-Kutta algorithm.

Acknowledgments

Computations were performed on the CRAY94, CRAY98 and NEC machines of the Institut du Développement et des Ressources en Informatique Scientifique and on the facilities of the Program “Simulations Interactives et Visualisation en Astronomie et Mécanique” at the Observatoire de la Côte d’Azur. This work was supported in part by the “Programme National Soleil Terre” of the CNRS and by NSF Grant No. PHY94-07194.

References

1. J.D. Huba, *Phys. Plasmas* **2**, 2504 (1995).
2. V.C.A. Ferraro, *Proc. R. Soc. London* Ser. A **233**, 310 (1955).
3. S.R. Spangler, in *Nonlinear Waves and Chaos in Space Plasmas*, 171, eds. T. Hada and H. Matsumoto (Terra Scientific, Tokyo, 1997).
4. C. Sulem and P.L. Sulem, *The Nonlinear Schrödinger Equation*, Applied Mathematical Sciences **139** (Springer-Verlag, 1999).
5. P.K. Shukla and L. Stenflo, *Space Sci.* **155**, 145 (1989).
6. S. Champeaux, T. Passot, and P.L. Sulem, *J. Plasma Phys.*, **58**, 665 (1997).
7. S. Champeaux, A. Gazol, T. Passot, and P.L. Sulem, in *Nonlinear MHD Waves and Turbulence*, eds T. Passot and P.L. Sulem, Lecture Notes in Physics **536**, 54 (Springer-Verlag, 1999).
8. T. Passot and P.L. Sulem, *Phys. Rev. E* **48**, 2966 (1993).
9. A. Gazol, T. Passot, and P.L. Sulem, *Phys. Plasmas*, **6**, 3114 (1999).
10. A. Rogister, *Phys. Fluids* **14**, 2733 (1971).
11. K. Mio, T. Ogino, K. Minami, and S. Takeda, *Phys. Soc. Japan* **41**, 265 (1975).
12. E. Mjølhus, *J. Plasma Phys.* **16**, 321 (1976).
13. C.F. Kennel, B. Buti, T. Hada, and R. Pellat, *Phys. Fluids* **31**, 1949 (1988).
14. E. Mjølhus and T. Hada in *Nonlinear Waves and Chaos in Space Plasmas*, 121, eds. T. Hada and H. Matsumoto (Terra Scientific, Tokyo, 1997).
15. D. Laveder, T. Passot, and P.L. Sulem, Transverse collapse of low-frequency Alfvén waves, to appear in *Physica D.*
16. S. Champeaux, D. Laveder, T. Passot, and P.L. Sulem, *Nonlin. Proc. Geophys.* **6**, 169 (1999).
17. H.K. Wong and M.L. Goldstein, *J. Geophys. Res.* **91**, 5617 (1986).
18. D.J. Kaup and A.C. Newell, *J. Math. Phys.* **19**, 798 (1978).
19. D. Laveder, T. Passot, and P.L. Sulem, Three-dimensional dynamics of Alfvén waves, preprint.
20. K.V. Roberts and J.B. Taylor, *Phys. Rev. Lett.* **8**, 197 (1962).
21. V.A. Marchenko, R.D. Denton, M.K. Hudson, *Phys. Plasmas* **3**, 3861 (1996).
22. E. Mjølhus and J. Wyller, *J. Plasma Phys.* **40**, 299 (1988).
23. S.R. Spangler, *Phys. Fluids* B **2**, 407 (1990).
24. M.V. Medvedev and P.H. Diamond, *Phys. Plasmas* **3**, 863 (1995).
25. C. Canuto, Y. Hussaini, A. Quateroni, and T. A. Zang, *Spectral Methods in Fluid Dynamics* (Springer Verlag, 1988).